J. Fluid Mech. (2003), *vol.* 474, *pp.* 319–337.
DOI: 10.1017/S0022112002002641 Printed in the United Kingdom

Computation of the pressure inside bubbles and pores in Stokes flow

By C. POZRIKIDIS

Department of Mechanical and Aerospace Engineering, University of California, San Diego, La Jolla, CA 92093-0411, USA
cpozrikidis@ucsd.edu

(Received 27 March 2002 and in revised form 2 August 2002)

Numerical methods are discussed for computing the pressure inside a two- or three-dimensional inviscid bubble with negligible density suspended in Stokes flow, subject to a specified rate of expansion. In the case of flow past a solitary two- or three-dimensional bubble, the bubble pressure is found by solving an integral equation of the first kind for the normal derivative of the pressure on the side of the liquid over the free surface, while requiring that the pressure field decays at a rate that is faster than the potential due to a point source. In another approach, an explicit expression for the bubble pressure is derived by applying the reciprocal theorem for the flow around the bubble and the flow due to a point source situated inside the bubble. In the case of flow past, or due to the expansion or shrinkage of, a periodic lattice of bubbles, the bubble pressure is found by solving an integral equation of the second kind for the density of an interfacial distribution of point-source dipoles, while ensuring existence and uniqueness of solution by spectrum deflation. The new methods considerably simplify the computation of the bubble pressure by circumventing the evaluation of the finite part of hypersingular integrals. Results of numerical simulations illustrate the pressure developing inside a solitary two- and three-dimensional incompressible bubble suspended in simple shear flow, and the pressure developing inside a doubly periodic array of gaseous inclusions representing shrinking pores trapped in a sintered medium.

1. Introduction

In a recent paper, the author discussed the pressure developing inside a solitary two-dimensional incompressible bubble suspended in Stokes flow, and the expansion or shrinkage of a compressible bubble whose area changes arbitrarily or as a function of the bubble pressure according to a specified equation of state (Pozrikidis 2001*a*). Results of numerical computations showed that the pressure inside a two-dimensional incompressible bubble that is suddenly subjected to pure elongational or simple shear flow increases, passes through a maximum, and finally decreases toward an asymptotic value as the bubble approaches the steady state. The asymptotic value was in excellent agreement with Richardson's (1968) analytical predictions for the bubble pressure at steady state. Correspondingly, the area of a compressible bubble occupied by a gas that obeys the usual equation of state of the form $p_B A_B^{\lambda} = f(T)$ decreases, passes through a minimum, and then increases toward an asymptotic value as the bubble approaches the steady state; p_B is the bubble pressure, A_B is the bubble area, λ is a positive exponent, and $f(T)$ is a function of temperature. Crowdy (2003*a*)

independently confirmed these results using the complex-variable formulation of two-dimensional Stokes flow. In his approach, the problem is conveniently formulated in terms of a finite set of coupled nonlinear ordinary differential equations, but only for a certain class of initial shapes.

In the earlier study (Pozrikidis 2001*a*), the bubble pressure was computed by evaluating the finite part of hypersingular integrals that arise from the boundary-integral formulation of Stokes flow. Unfortunately, the extension of this method to three-dimensional flow past a solitary bubble and to two- or three-dimensional flow past or due to the expansion or shrinkage of bubbles arranged on a periodic lattice is cumbersome. The periodic flow is of particular interest in studies of foam expansion or inclusion shrinkage occurring in the process of sintering (e.g. Pozrikidis 2002*a*; Crowdy 2003*b*). In the case of three-dimensional flow, the evaluation of hypersingular integrals requires strong smoothness conditions that disqualify the usage of general-purpose boundary-element methods for interfacial flow. In the case of periodic flow, the boundary-integral formulation for the pressure is frustrated by unwieldy pressure kernels associated with the periodic stresslet.

These difficulties have motivated the reconsideration of the problem of computing the bubble pressure in Stokes flow with the goal of developing a numerical method that is applicable to general flow configurations. The new approach hinges on the realization that the pressure field in Stokes flow satisfies Laplace's equation, and may thus be described using either Green's third identity or a generalized representation involving an interfacial distribution of point-source dipoles. An additional distinguishing condition that allows the computation of the pressure must be imposed according to the particular flow configuration, and it emerges by requiring that the integral equations obtained from the integral representation admit a unique and properly behaving solution. A second approach uses the reciprocal theorem for Stokes flow applied to the particular flow of interest and the flow due to a point source situated inside the bubble to derive an explicit expression for the bubble.

In this paper, the development and implementation of the new methodology is demonstrated for three prototypical flows. In § 2, we consider the pressure developing inside a two-dimensional solitary bubble in simple shear flow and confirm that the results are in agreement with those obtained using the earlier method. In § 3, we consider the pressure developing inside a three-dimensional solitary bubble in shear flow and find similarities with the case of two-dimensional flow. In § 4, we consider the pressure developing inside a doubly periodic array of shrinking two-dimensional bubbles. Straightforward extensions of these fundamental case studies allow us to tackle arbitrary configurations of two- and three-dimensional Stokes flow.

2. Computation of the bubble pressure in two-dimensional flow

Consider simple shear flow past a solitary two-dimensional inviscid bubble with negligible density in the limit of vanishing Reynolds number, as illustrated in figure 1(*a*). The gas–liquid interface is assumed to be a free surface with uniform surface tension γ. The hydrodynamic traction along the free surface on the side of the liquid is given by

$$\boldsymbol{f} \equiv \boldsymbol{\sigma} \cdot \boldsymbol{n} = (-p_B + \gamma\kappa)\boldsymbol{n}, \tag{2.1}$$

where $\boldsymbol{\sigma}$ is the Newtonian stress tensor, $\boldsymbol{n}$ is the unit vector normal to the free surface pointing into the liquid, p_B is the bubble pressure, and κ is the curvature of the free surface in the (x, y)-plane; for a circular bubble of radius a, $\kappa = 1/a$. Decomposing

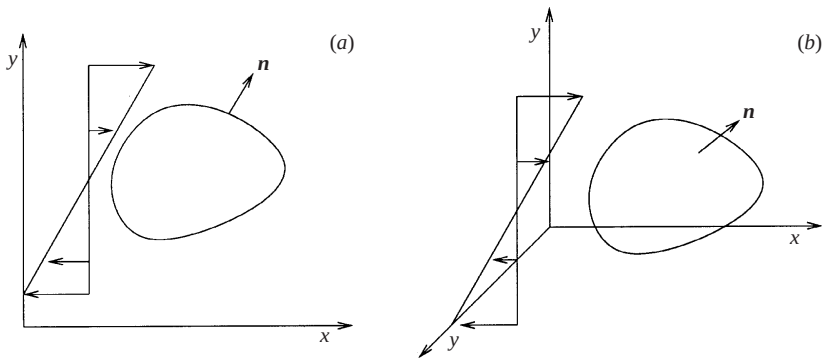

FIGURE 1. Illustration of simple shear flow along the x-axis past (a) a two-dimensional and (b) a three-dimensional bubble.

the normal stress into its pressure and viscous components, and using the continuity equation to express the viscous component in terms of the tangential derivative of the velocity projected onto the tangential vector along the bubble surface, we obtain

$$p = p_B - 2\mu \frac{\partial \boldsymbol{u}}{\partial l} \cdot \boldsymbol{t} - \gamma\kappa, \tag{2.2}$$

where $\boldsymbol{t}$ is the unit vector tangent to the free surface pointing in the direction of increasing arc length l.

2.1. *Green's third identity for the pressure*

Recall now that the pressure in Stokes flow is a harmonic function, and use Green's third identity to express the pressure at the point $\boldsymbol{x}_0$ that lies in the liquid in the integral form

$$p(\boldsymbol{x}_0) = p_\infty - \int_C G^L(\boldsymbol{x}, \boldsymbol{x}_0) \frac{\partial p(\boldsymbol{x})}{\partial n} \, \mathrm{d}l(\boldsymbol{x}) + \int_C p(\boldsymbol{x}) [\boldsymbol{n}(\boldsymbol{x}) \cdot \nabla G^L(\boldsymbol{x}, \boldsymbol{x}_0)] \, \mathrm{d}l(\boldsymbol{x}), \tag{2.3}$$

where $\partial p/\partial n \equiv \boldsymbol{n}(\boldsymbol{x}) \cdot \nabla p(\boldsymbol{x})$ is the normal derivative of the pressure, C is the free surface, p_∞ is the pressure at infinity, $G^L(\boldsymbol{x}, \boldsymbol{x}_0) = -(1/2\pi) \ln r/c$ is the free-space Green's function of Laplace's equation in two dimensions, $r \equiv |\boldsymbol{x} - \boldsymbol{x}_0|$, and c is an arbitrary positive constant with dimensions of length. Taking the limit of (2.3) as the evaluation point $\boldsymbol{x}_0$ approaches the free surface, expressing the limit of the double-layer potential in terms of its principal value, substituting the right-hand side of (2.2) for the free-surface pressure, and rearranging, we find

$$\int_C G^L(\boldsymbol{x}, \boldsymbol{x}_0) \frac{\partial p(\boldsymbol{x})}{\partial n} \, \mathrm{d}l(\boldsymbol{x}) + p_B = p_\infty + \tfrac{1}{2} q(\boldsymbol{x}_0) - \int_C^{PV} q(\boldsymbol{x}) [\boldsymbol{n}(\boldsymbol{x}) \cdot \nabla G^L(\boldsymbol{x}, \boldsymbol{x}_0)] \, \mathrm{d}l(\boldsymbol{x}), \tag{2.4}$$

where PV denotes the principal-value integral, and we have defined $p = p_B - q$ and

$$q(\boldsymbol{x}) \equiv 2\mu \left(\frac{\partial \boldsymbol{u}}{\partial l} \cdot \boldsymbol{t} \right) (\boldsymbol{x}) + \gamma\kappa(\boldsymbol{x}). \tag{2.5}$$

Given the instantaneous bubble shape and tangential velocity along the free surface, (2.4) provides us with an integral equation of the first kind for the normal derivative of the pressure. The bubble pressure on the left-hand side of (2.4) is an unknown that must be computed as part of the solution by introducing a scalar constraint.

Alternatively, we may use the integral formulation of Stokes flow to express the pressure in terms of the interfacial traction and velocity in the form

$$p(\boldsymbol{x}_0) = p_\infty - \frac{1}{4\pi}\int_C f_i(\boldsymbol{x}) P_i(\boldsymbol{x}_0,\boldsymbol{x})\,\mathrm{d}l(\boldsymbol{x}) + \frac{\mu}{4\pi}\int_C u_i(\boldsymbol{x}) \Pi_{ik}(\boldsymbol{x}_0,\boldsymbol{x}) n_k(\boldsymbol{x})\,\mathrm{d}l(\boldsymbol{x}), \tag{2.6}$$

where the kernels P_i and Π_{ik} are the pressure fields associated with the point force and the stresslet. For flow in free space, these are given by

$$P_i(\boldsymbol{x}_0,\boldsymbol{x}) = -2\frac{\partial \ln r}{\partial \hat{x}_i} = -2\frac{\hat{x}_i}{r^2}, \tag{2.7a}$$

$$\Pi_{ik}(\boldsymbol{x}_0,\boldsymbol{x}) = -4\frac{\partial^2 \ln r}{\partial \hat{x}_i \partial \hat{x}_k} = -4\left(\frac{\delta_{ik}}{r^2} - 2\frac{\hat{x}_i \hat{x}_k}{r^4}\right), \tag{2.7b}$$

where $\hat{\boldsymbol{x}} = \boldsymbol{x} - \boldsymbol{x}_0$ and $r = |\hat{\boldsymbol{x}}|$. Taking the limit of (2.6) as the evaluation point $\boldsymbol{x}_0$ approaches the free surface, and manipulating the emerging 'hypersingular' integrals by subtracting the strong singularities of the kernels (Pozrikidis 2001*a*), we find that the pressure on the side of the liquid is given by the regularized integral representation

$$\begin{aligned} p(\boldsymbol{x}_0) = p_\infty &+ \frac{\gamma}{2\pi}\int_C n_i(\boldsymbol{x})\frac{x_i - x_{0_i}}{r^2}[\kappa(\boldsymbol{x}) - \kappa(\boldsymbol{x}_0)]\,\mathrm{d}l(\boldsymbol{x}) \\ &+ \frac{2\mu}{\pi}\int_C [u_i(\boldsymbol{x}) - u_i(\boldsymbol{x}_0)]\frac{\hat{x}_i \hat{x}_k}{r^4} n_k(\boldsymbol{x})\,\mathrm{d}l(\boldsymbol{x}) \\ &- \frac{\mu}{\pi}\int_C^{PV} [u_i(\boldsymbol{x}) - u_i(\boldsymbol{x}_0)]\frac{n_i(\boldsymbol{x})}{r^2}\,\mathrm{d}l(\boldsymbol{x}) - \mu\left(\frac{\partial u_i}{\partial l}\right)(\boldsymbol{x}_0) t_i(\boldsymbol{x}_0), \end{aligned} \tag{2.8}$$

where $\boldsymbol{x}_0$ lies on the free surface C. The first two integrals on the right-hand side of (2.8) are non-singular, whereas the third is a Cauchy principal-value integral. Pozrikidis (2001*a*) used the integral representation (2.8) in conjunction with the interfacial condition (2.2) to evaluate the liquid pressure and the bubble pressure at marker points distributed along the free surface, and then averaged the pointwise results to eliminate numerical oscillations and improve the accuracy.

The representation (2.6) shows that, far from the free surface, the pressure behaves like

$$p(\boldsymbol{x}_0) \simeq p_\infty - P_i(\boldsymbol{x}_0,\boldsymbol{x}_c)\frac{1}{4\pi}\int_C f_i(\boldsymbol{x})\,\mathrm{d}l(\boldsymbol{x}) + O\left(\frac{1}{r^2}\right), \tag{2.9}$$

where $\boldsymbol{x}_c$ is a designated bubble centre. Because the force exerted on the bubble vanishes, as required by the equilibrium equation (2.1), the integral on the right-hand side of (2.9) is zero, and the disturbance pressure field decays like $1/r^2$. This observation provides us with a condition for the computation of p_B in conjunction with the integral equation (2.4),

$$\int_C \frac{\partial p(\boldsymbol{x})}{\partial n}\,\mathrm{d}l(\boldsymbol{x}) = 0, \tag{2.10}$$

which ensures that the pressure field decays faster than the potential due to a point source. The main advantage of this approach is that the computation of the bubble pressure requires the evaluation of weakly singular and non-singular principal-value integrals. In contrast, the last three terms of the right-hand side of (2.8) define the 'finite part' or 'Hadamard value' of a hypersingular integral. The advantage of the present formulation is marginal in the case of two-dimensional flow past a solitary

bubble discussed in this section, but significant in the case of three-dimensional flow and periodic two- or three-dimensional flow discussed in §§ 3 and 4.

It is known that the solution of the integral equation of the first kind (2.4) for $\partial p/\partial n$ with the free-space Green's function is unique only when the transfinite radius of the contour C is not equal to the constant c involved in the definition of the Green's function (Yan & Sloan 1988) – the transfinite radius of a circle is equal to its radius. If this condition is not satisfied, any particular solution can be modified with the addition of an arbitrary constant. The integral constraint (2.10) removes this freedom and renders the solution unique for any free-surface shape and size.

A standard boundary-element collocation method was implemented for solving the integral equation (2.4) accompanied by (2.10). The function q defined in (2.5) and the normal derivative of the pressure were approximated with linear functions over the boundary elements, and the system of linear equations was solved by Gauss elimination. The method was applied to compute the evolution of the pressure inside an incompressible bubble deforming under the action of a simple shear flow, $\boldsymbol{u}^{\infty} = (ky, 0)$, where k is the shear rate, for a broad range of capillary numbers $Ca = \mu ka/\gamma$, where a is the radius of the circular bubble. The results were in excellent agreement with those obtained by the previous method (Pozrikidis 2001*a*), as well as with Richardson's (1968) analytical predictions for the bubble pressure at steady state. New results include the distribution of the normal derivative of the pressure along the bubble surface during the evolution.

Richardson (1968) showed that steady elliptical bubble shapes exist for any capillary number. The higher the capillary number, that is the higher the shear rate, the larger the aspect ratio and the smaller the inclination of the deformed bubble with respect to the direction of the unperturbed shear flow. Figure 2(*a*, *b*) shows stages in the deformation of an incompressible bubble from the circular initial shape for $Ca = 0.10$ and 0.50, at times $kt = 0$, 0.25, 0.5, 0.75. 1.0 and 5.0, computed using the boundary-element method discussed by Pozrikidis (2001*a*). Figure 2(*c*, *d*) shows the corresponding distributions of the dimensionless normal derivative of the pressure $\chi \equiv a(\partial p/\partial n)/(k\mu)$, plotted against the polar angle θ measured around the bubble centre; the sinusoidal lines correspond to the initial circular shape. The results show that the normal derivative of the pressure, proportional to the tangential derivative of the vorticity, develops a sharp peak at the tip of the deformed bubble.

Figure 3 shows the evolution of the reduced bubble pressure, defined as $\delta\hat{p}_B \equiv (p_B - p_\infty - \gamma/a)/(\mu k)$, for $Ca = 0.10$, 0.3 and 0.5. The solid lines were produced by solving the integral equation (2.4), and the dotted lines were produced by evaluating the pressure at the interfacial nodes using the strongly singular integral representation (2.6), and then computing the average to eliminate numerical oscillation. The good agreement confirms the consistency of the present approach.

2.2. *The reciprocal theorem with a point source*

The velocity field due to a two-dimensional point source of unit strength placed at the point $\boldsymbol{x}_s$ is given by $u_i^s = \hat{x}_i/(2\pi r^2) = -P_i/(4\pi)$, where $\hat{\boldsymbol{x}} = \boldsymbol{x} - \boldsymbol{x}_s$, $r \equiv |\hat{\boldsymbol{x}}|$, and the vector P_i is defined in (2.7*a*). This irrotational field satisfies the equations of Stokes flow with an associated uniform pressure which, for convenience and without loss of generality, can be set equal to zero. The corresponding stress field is given by $\sigma_{ij}^s = -\mu\Pi_{ij}/(4\pi)$, where the tensor Π_{ij} is defined in (2.7*b*).

Placing the singular point $\boldsymbol{x}_s$ inside the bubble, and applying the reciprocal theorem

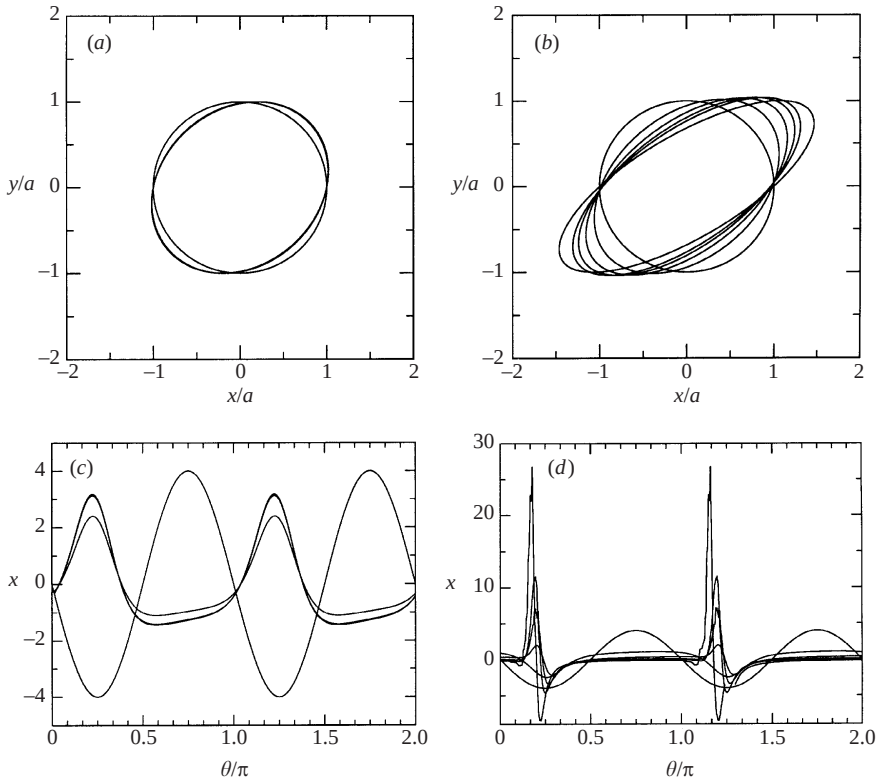

FIGURE 2. (a, b) Stages in the deformation of an incompressible bubble for (a) $Ca = 0.10$ and (b) 0.50, at times $kt = 0$, 0.25, 0.5, 0.75. 1.0, and 5.0. (c, d) Corresponding distributions of the reduced normal derivative of the pressure χ plotted against the polar angle θ measured around the bubble centre; the sinusoidal lines correspond to the initial circular shape.

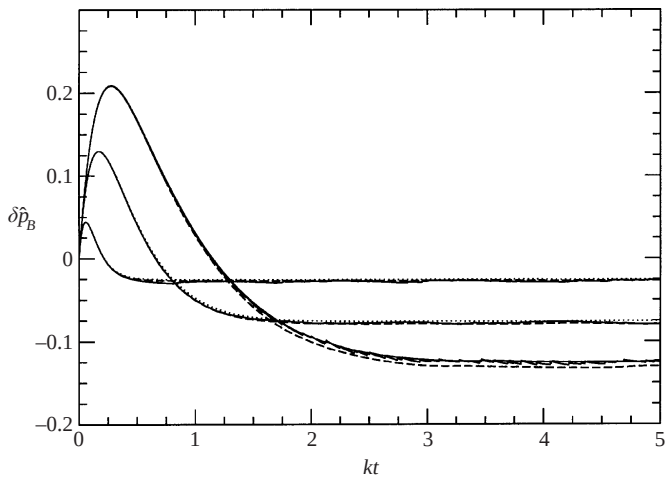

FIGURE 3. Reduced pressure developing inside a two-dimensional incompressible bubble, $\delta\hat{p}_B \equiv (p_B - p_\infty - \gamma/a)/(\mu k)$, for $Ca = 0.1$, 0.3, and 0.5 (highest curve). The solid lines were generated by solving the integral equation (2.4), the dotted lines were generated by evaluating the pressure at the interfacial nodes using the strongly singular integral representation (2.6), and the dashed lines were generated by evaluating the right-hand side of (2.13).

for the Stokes flow past the bubble and the flow due to the point source, we find

$$\int_C u_i(\boldsymbol{x})\sigma^s_{ik}(\hat{\boldsymbol{x}})n_k(\boldsymbol{x})\,\mathrm{d}l(\boldsymbol{x}) = \int_C u^s_i(\hat{\boldsymbol{x}})\sigma_{ik}(\boldsymbol{x})n_k(\boldsymbol{x})\,\mathrm{d}l(\boldsymbol{x}) + p_\infty, \tag{2.11}$$

where C is the bubble contour. The pressure at infinity arises from the limiting value of the integral shown on the right-hand side (2.11) computed over a large contour enclosing the bubble; the corresponding integral shown on the left-hand side vanishes. Replacing the free-surface traction with the right-hand side of (2.1) and rearranging, we obtain an explicit expression for the bubble pressure,

$$p_B = p_\infty + \gamma \int_C u^s_i(\hat{\boldsymbol{x}})n_i(\boldsymbol{x})\kappa(\boldsymbol{x})\,\mathrm{d}l(\boldsymbol{x}) - \int_C u_i(\boldsymbol{x})\sigma^s_{ik}(\hat{\boldsymbol{x}})n_k(\boldsymbol{x})\,\mathrm{d}l(\boldsymbol{x}), \tag{2.12}$$

which can be recast into the form

$$p_B = p_\infty - \frac{\gamma}{4\pi}\int_C P_i(\hat{\boldsymbol{x}})n_i(\boldsymbol{x})\kappa(\boldsymbol{x})\,\mathrm{d}l(\boldsymbol{x}) + \frac{\mu}{4\pi}\int_C u_i(\boldsymbol{x})\Pi_{ik}(\hat{\boldsymbol{x}})n_k(\boldsymbol{x})\,\mathrm{d}l(\boldsymbol{x}). \tag{2.13}$$

In the case of a circular bubble suspended in a quiescent ambient fluid, equation (2.13) produces the expected result $p_B = p_\infty + \gamma\kappa$. More generally, once the interfacial velocity is available, the integrals on the right-hand side of (2.13) can be computed by standard numerical methods.

Working in a similar fashion, we find that, if the point source is placed inside the liquid, the reciprocal theorem applied for the point source leads us to the integral representation (2.6) stated earlier on the basis of the integral representation for the velocity. In this sense, (2.13) is a natural companion of (2.6).

The dashed lines in figure 3 were produced by evaluating the right-hand side of (2.13) with the point source located at the bubble centre. The results show that this method of evaluating the bubble pressure is somewhat more accurate than the other two methods, although the accuracy does depend on the precise location of the point source.

2.3. *Evolution of a compressible bubble*

In practical applications, the bubble pressure is either specified in absolute terms or related to the bubble volume and temperature by means of an equation of state. In these cases, the rate of bubble expansion, Q, is an unknown that must be found as part of the solution. Pozrikidis (2001*a*) implemented a method of computing Q based on the observation that, in Stokes flow, Q is linear function of the bubble pressure.

An alternative method would be to supplement the equations of Stokes flow with the integral constraint (2.13). In the implementation of the boundary-integral method, this constraint is expressed in the form of the scalar linear functional $F(p_B, \boldsymbol{u}) = 0$, and the term $F(p_B, \boldsymbol{u})\boldsymbol{v}(\boldsymbol{x})$ is added to the integral equation of the second kind for the interfacial velocity, where $\boldsymbol{v}(\boldsymbol{x})$ is an arbitrary vector function that is non-orthogonal to the normal vector $\boldsymbol{n}$, that is, $\int_C v_i n_i\,\mathrm{d}l \neq 0$; a simple choice is $\boldsymbol{v} = \boldsymbol{n}$. Straightforward analysis shows that the solution of the modified integral equation will satisfy the requisite constraint (2.13).

3. Computation of the bubble pressure in three-dimensional flow

The new formulation is especially useful in the case of three-dimensional flow past a solitary bubble illustrated in figure 1(*b*), where the evaluation of hypersingular integrals associated with the integral representation for the pressure is extremely

sensitive to the discretization error. Repeating the analysis of § 2 with straightforward changes in notation, we derive the counterpart of the integral equation (2.4) originating from Green's third identity

$$\int_D G^L(\boldsymbol{x},\boldsymbol{x}_0)\frac{\partial p(\boldsymbol{x})}{\partial n}\,\mathrm{d}S(\boldsymbol{x})+p_B = p_\infty+\tfrac{1}{2}q(\boldsymbol{x}_0)-\int_D^{PV} q(\boldsymbol{x})[\boldsymbol{n}(\boldsymbol{x})\cdot\nabla G^L(\boldsymbol{x},\boldsymbol{x}_0)]\,\mathrm{d}S(\boldsymbol{x}), \quad (3.1)$$

where D is the bubble surface, $G^L(\boldsymbol{x},\boldsymbol{x}_0) = 1/(4\pi r)$, is the free-space Green's function of Laplace's equation in three dimensions, $r \equiv |\boldsymbol{x}-\boldsymbol{x}_0|$, and PV denotes the principal-value integral. The surface function q is defined as

$$q(\boldsymbol{x}) \equiv 2\mu\,\theta_S + 2\gamma\kappa_m(\boldsymbol{x}), \quad (3.2)$$

where κ_m is the mean curvature,

$$\theta_S \equiv \mathrm{Trace}[\boldsymbol{P}\cdot(\nabla\boldsymbol{u})\cdot\boldsymbol{P}] \quad (3.3)$$

is the rate of surface dilatation, $\boldsymbol{P} = \boldsymbol{I} - \boldsymbol{nn}$ is the tangential projection operator, and $\boldsymbol{I}$ is the unit matrix. If ξ and η comprise a pair of surface curvilinear coordinates with associated surface metric h_S, then θ_S may be expressed in the computationally convenient form

$$\theta_S = \frac{1}{h_s}\boldsymbol{n}\cdot\left(\frac{\partial\boldsymbol{u}}{\partial\xi}\times\frac{\partial\boldsymbol{x}}{\partial\eta}+\frac{\partial\boldsymbol{x}}{\partial\xi}\times\frac{\partial\boldsymbol{u}}{\partial\eta}\right). \quad (3.4)$$

Alternatively, we may use the integral formulation of Stokes flow to express the pressure in terms of the interfacial velocity in the form

$$p(\boldsymbol{x}_0) = p_\infty - \frac{1}{8\pi}\int_D f_i(\boldsymbol{x})P_i(\boldsymbol{x}_0,\boldsymbol{x})\,\mathrm{d}S(\boldsymbol{x}) + \frac{\mu}{8\pi}\int_D u_i(\boldsymbol{x})\Pi_{ik}(\boldsymbol{x}_0,\boldsymbol{x})n_k(\boldsymbol{x})\,\mathrm{d}S(\boldsymbol{x}), \quad (3.5)$$

where the kernels P_i and Π_{ik} are the pressure fields associated with the three-dimensional point force and stresslet. For infinite flow in free space, these are given by

$$P_i(\boldsymbol{x}_0,\boldsymbol{x}) = 2\frac{\partial}{\partial\hat{x}_i}\left(\frac{1}{r}\right) = -2\frac{\hat{x}_j}{r^3}, \quad (3.6a)$$

$$\Pi_{ik}(\boldsymbol{x}_0,\boldsymbol{x}) = -4\frac{\partial^2}{\partial x_i\partial x_k}\left(\frac{1}{r}\right) = -4\left(\frac{\delta_{ik}}{r^3}-3\frac{\hat{x}_i\hat{x}_k}{r^5}\right). \quad (3.6b)$$

Taking the limit of the integral representation (3.5) as the evaluation point $\boldsymbol{x}_0$ approaches the free surface produces unwieldy 'hypersingular' integrals.

The representation (3.5) requires that the normal derivative of the pressure satisfy the counterpart of the integral constraint (2.10)

$$\int_D \frac{\partial p(\boldsymbol{x})}{\partial n}\,\mathrm{d}S(\boldsymbol{x}) = 0, \quad (3.7)$$

which serves as a distinguishing condition for the computation of the bubble pressure.

Although a rigorous proof is not available, lack of evidence to the contrary suggests that the integral equation of the first kind for $\partial p/\partial n$ with the free-space Green's function shown in (3.1) has a unique solution, in contrast to its two-dimensional counterpart (e.g. Nédélec & Planchard 1973). This important difference can be attributed, in part, to the positiveness of the three-dimensional Green's function of Laplace's equation. In contrast, the two-dimensional Green's function is positive when $r > c$

and negative otherwise, where c is the constant length involved in the definition of the Green's function.

The counterpart of the integral representation (2.13) is

$$p_B = p_\infty - \frac{\gamma}{4\pi}\int_D P_i(\hat{\boldsymbol{x}})n_i(\boldsymbol{x})\kappa_m(\boldsymbol{x})\,\mathrm{d}S(\boldsymbol{x}) + \frac{\mu}{8\pi}\int_D u_i(\boldsymbol{x})\Pi_{ik}(\hat{\boldsymbol{x}})n_k(\boldsymbol{x})\,\mathrm{d}S(\boldsymbol{x}), \tag{3.8}$$

where $\hat{\boldsymbol{x}} \equiv \boldsymbol{x} - \boldsymbol{x}_s$, and the singular point $\boldsymbol{x}_s$ is located inside the bubble. The integrals on the right-hand side of (3.8) may be computed by standard numerical methods.

A standard boundary-element collocation method was implemented for computing the evolution of the bubble and solving the integral equation (3.1) subject to the integral constraint (3.7) (e.g. Pozrikidis 2001*c*). In the numerical implementation, the bubble surface was discretized into an unstructured surface grid of six-node triangular elements generated from the successive subdivisions of a regular octahedron, and all surface functions were approximated with quadratic functions with respect to the local triangle coordinates (e.g. Pozrikidis 2002*b*). The influence matrix associated with the single-layer harmonic potential on the left-hand side of (3.1) was generated by the method of impulses, and the linear system resulting from node collocation was solved by Gauss elimination. For the finest discretization considered, involving 512 elements and 1026 interfacial nodes, each evaluation of the bubble pressure requires approximately 10 minutes of CPU time on an INTEL 1.7 GHz processor running Linux.

Figure 4 shows the evolution of the excess pressure developing inside an incompressible bubble subjected to a impulsively started simple shear flow, for a low and a moderate capillary number $Ca \equiv \mu k a/\gamma = 0.2$ and 0.5; a is the radius of the spherical bubble. The simulation ended when the computation could no longer be continued with adequate accuracy due to significant grid distortion. The symbols in figure 4 represent results obtained using the numerical method discussed in the previous paragraph, and the solid lines represent results obtained by evaluating the right-hand side of (3.8) with the point source located at the bubble centre. For both capillary numbers, the bubble deforms and reaches a steady state at long times. The numerical error in the computation of the bubble pressure is estimated to be on the order of $0.01\,\mu k$. Although the numerical accuracy is marginally adequate and the length of the simulation is limited by the deformation of the surface grid, figure 4 nevertheless provides compelling evidence that a maximum in the pressure develops during the evolution, similar to that displayed in figure 3 for two-dimensional flow.

4. Expansion and shrinkage in two-dimensional doubly periodic flow

Consider now the flow induced by the expansion or shrinkage of a doubly periodic array of two-dimensional bubbles arranged on a square or hexagonal lattice, as illustrated in figure 5. The doubly periodic configuration can be regarded as a model of an ordered expanding foam or an array of shrinking inclusions developing during the late stages of viscous sintering. In the periodic model, the bubbles are deployed at the vertices of a two-dimensional lattice defined by the base vectors $\boldsymbol{a}^{(1)}$ and $\boldsymbol{a}^{(2)}$, as depicted in figure 5. For the square lattice $\boldsymbol{a}^{(1)} = [L(t), 0]$ and $\boldsymbol{a}^{(2)} = [0, L(t)]$, and for the hexagonal lattice $\boldsymbol{a}^{(1)} = [L(t), 0]$ and $\boldsymbol{a}^{(2)} = [\frac{1}{2}L(t), \frac{1}{2}\sqrt{3}L(t)]$, where $L(t)$ is the evolving length of the lattice side. In both expansion and shrinkage, the structure of the lattice is assumed to be preserved, and the pressure field in the liquid is required to be periodic in the directions of the two base vectors.

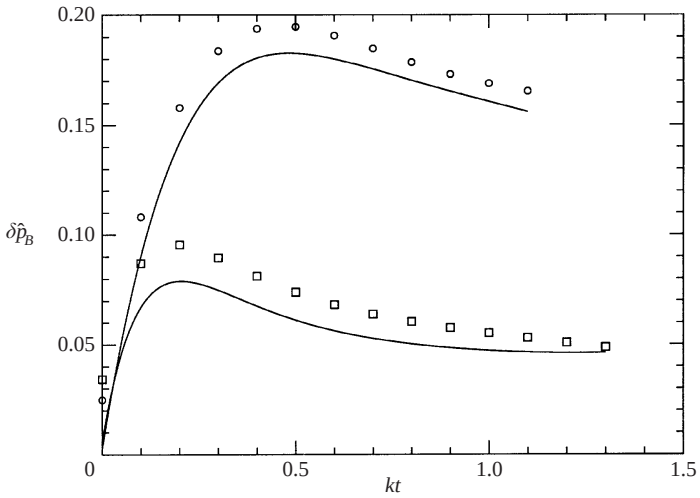

FIGURE 4. Reduced pressure developing inside a three-dimensional incompressible bubble, $\delta\hat{p}_B \equiv (p_B - p_\infty - 2\gamma/a)/(\mu k)$, for $Ca = 0.2$ (squares) and 0.5 (circles). The solid lines represent results obtained by evaluating the right-hand side of (3.8).

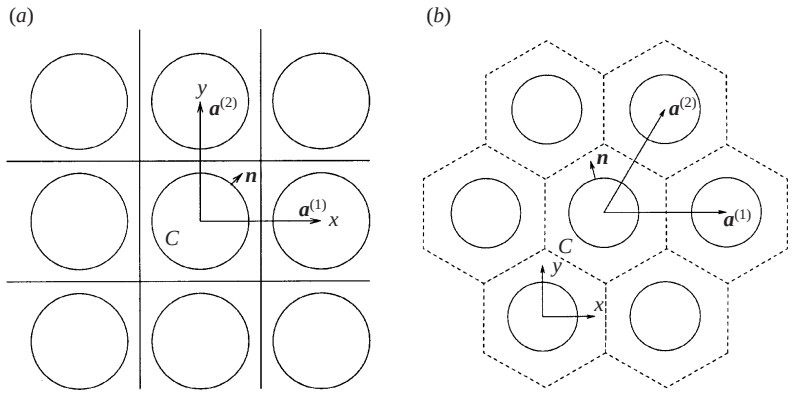

FIGURE 5. Expansion or shrinkage of a doubly periodic array of two-dimensional bubbles or pores arranged on (*a*) a square or (*b*) a hexagonal lattice, representing an expanding foam or a sintering material.

4.1. *Dipole representation*

It is convenient to represent the pressure field in the liquid in terms of an interfacial distribution of point-source dipoles pointing normal to the free surfaces, amounting to a double-layer harmonic potential, in the form

$$p(\boldsymbol{x}_0) = p_0 - \int_C \varphi(\boldsymbol{x})[\boldsymbol{n}(\boldsymbol{x}) \cdot \boldsymbol{D}(\boldsymbol{x} - \boldsymbol{x}_0)]\, \mathrm{d}l(\boldsymbol{x}), \tag{4.1}$$

where p_0 is the liquid pressure in the absence of fluid motion, C is the contour of one bubble or pore, φ is the *a priori* unknown strength density of the dipoles, and $\boldsymbol{D}(\boldsymbol{x} - \boldsymbol{x}_0)$ is the harmonic field due to a doubly periodic array of dipoles. One of the dipoles is located at the point $\boldsymbol{x}_0 = (x_0, y_0)$, and the nth dipole is located at the point $\boldsymbol{x}^{(n)} = (x_n, y_n)$, where

$$x^{(n)} = x_0 + ia_x^{(1)} + ja_x^{(2)}, \qquad y^{(n)} = y_0 + ia_y^{(1)} + ja_y^{(2)}, \tag{4.2}$$

i and j are two integers, and the index n is defined in terms of the indices i and j by double summation.

Using the Ewald summation method, we find that the doubly periodic dipole can be expressed in the computationally convenient form

$$D_j(\boldsymbol{x}-\boldsymbol{x}_0) = \frac{1}{2A_c}(x_j - x_{0_j}) + \frac{1}{2\pi}\sum_n \frac{x_j - x_j^{(n)}}{r_n^2}\exp(-\hat{r}_n^2) + \frac{1}{A_c}\sum_m \frac{k_j^{(m)}}{k^{(m)^2}}\exp(-\tfrac{1}{4}\hat{k}^{(m)^2})\sin[\boldsymbol{k}^{(m)}\cdot(\boldsymbol{x}-\boldsymbol{x}_0)]. \tag{4.3}$$

The first sum on the right-hand side of (4.3) with respect to n runs over the dipole sites in physical space, while the second sum with respect to m runs over the vertices of the reciprocal lattice in wavenumber space. The base vectors of the reciprocal lattice are given by

$$\boldsymbol{b}^{(1)} = \frac{2\pi}{A_c}\boldsymbol{a}^{(2)}\times\boldsymbol{e}_z, \qquad \boldsymbol{b}^{(2)} = \frac{2\pi}{A_c}\boldsymbol{e}_z\times\boldsymbol{a}^{(1)}, \tag{4.4}$$

where $A_c = |\boldsymbol{a}^{(1)}\times\boldsymbol{a}^{(2)}|$ is the area of the unit cell in physical space. The vertices of the reciprocal lattice are located at $\boldsymbol{k}^{(m)} = (k_x^{(m)}, k_y^{(m)})$, where

$$k_x^{(m)} = ib_x^{(1)} + jb_x^{(2)}, \qquad k_y^{(m)} = ib_y^{(1)} + jb_y^{(2)}, \tag{4.5}$$

i and j are two integers, and the index m is defined in terms of i and j using double summation. The singular wavenumber corresponding to $i = 0$ and $j = 0$ is excluded from the second sum in (4.3). The rest of the symbols in (4.3) are defined as follows: $r_n = |\boldsymbol{x}-\boldsymbol{x}_n|$ is the distance of the evaluation point from the nth dipole, $\hat{r}_n = \xi r_n$ is the corresponding reduced dimensionless distance, $k^{(m)} = |\boldsymbol{k}^{(m)}|$ is the length of the mth wavenumber vector, $\hat{k}^{(m)} \equiv k^{(m)}/\xi$ is the reduced length of the mth wavenumber, and ξ is the Ewald splitting parameter with dimensions of inverse length, determining the balance of the sums in real and reciprocal space.

It can be shown, and it has been confirmed by numerical evaluation, that the right-hand side of (4.3) is independent of the selected value of ξ. As ξ tends to zero, we obtain a representation in terms of sums of real-space dipoles, whereas as ξ tends to infinity, we obtain a representation in terms of a double Fourier series in reciprocal wavenumber space. Both are added to a field that increases linearly in the direction of the dipoles, independent of the lattice geometry. This linear field was designed carefully so that the dipole vector satisfies the integral identity

$$\int_C \boldsymbol{n}(\boldsymbol{x})\cdot\boldsymbol{D}(\boldsymbol{x}-\boldsymbol{x}_0)\,\mathrm{d}l(\boldsymbol{x}) = \begin{cases} 1 & \text{when } \boldsymbol{x}_0 \text{ lies inside } C \\ \frac{1}{2} & \text{when } \boldsymbol{x}_0 \text{ lies on } C \\ 0 & \text{when } \boldsymbol{x}_0 \text{ lies outside } C, \end{cases} \tag{4.6}$$

where C is any closed contour in the (x, y)-plane, and the unit normal vector $\boldsymbol{n}$ points outward from C. When $\boldsymbol{x}_0$ lies on C, the principal value of the integral on the right-hand side of (4.6) is implied.

Taking the limit of (4.1) as the evaluation point $\boldsymbol{x}_0$ approaches the free surface C, expressing the limit of the double-layer integral in terms of its principal value, and requiring the interfacial condition (2.2), we derive an integral equation of the second

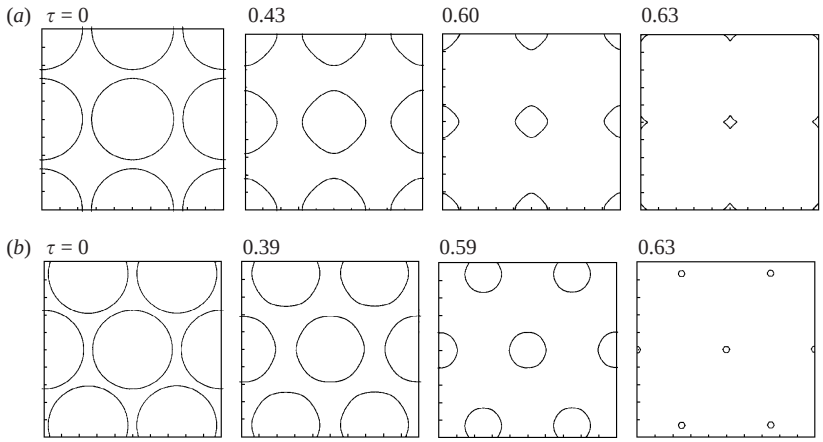

FIGURE 6. Shapes of bubbles shrinking at constant rate on (*a*) a square and (*b*) a hexagonal lattice for initial capillary number $Ca_0 = 1.0$.

kind for the strength density φ

$$\varphi(\boldsymbol{x}_0) = 2 \int_C^{PV} \varphi(\boldsymbol{x})[\boldsymbol{n}(\boldsymbol{x}) \cdot \boldsymbol{D}(\boldsymbol{x} - \boldsymbol{x}_0)] \, \mathrm{d}l(\boldsymbol{x}) + 2[p_B - q(\boldsymbol{x}_0) - p_0], \tag{4.7}$$

where the function q is defined in (2.5). The integral identity (4.6) implies that the integral equation (4.7) has either no solution or an infinite number of solutions that differ by an arbitrary constant. To remove this difficulty, we observe that the presence of the unspecified bubble pressure on the right-hand side allows us to deflate the spectrum of the integral operator and solve a perfectly well-posed problem. Accordingly, and to preserve linearity, we require that the bubble pressure is given by

$$p_B = \frac{\beta}{L_C} \int_C \varphi(\boldsymbol{x}) \, \mathrm{d}l(\boldsymbol{x}), \tag{4.8}$$

where L_C is the arc length of the contour C, and β is a non-zero but otherwise arbitrary dimensionless constant. Equation (4.7) supplemented with condition (4.8) may be solved using a standard boundary-element collocation method.

Figure 6(*a*) shows stages in the shrinkage of a doubly periodic array of initially circular bubbles arranged on a square lattice, contracting at a constant negative rate of shrinkage $Q = \mathrm{d}A_B/\mathrm{d}t$, where A_B is the area of one bubble. The bubble shapes are displayed in the plane of dimensionless axes $[x/L(t), y/L(t)]$, where the length of the lattice side $L(t)$ decreases appropriately during the evolution. The labels above the panels show the corresponding dimensionless times $\tau \equiv L_0^2 t/|Q|$, where L_0 is the initial lattice side. The initial bubble radius is $a_0 = 0.45L_0$, and the initial capillary number is $Ca_0 \equiv \mu|Q|/L_0\gamma = 1$. Figure 6(*b*) shows the corresponding evolution of bubbles arranged on a hexagonal lattice. The evolution of the free surfaces shown in figure 6 was computed using the boundary-integral method discussed in the Appendix, using 128 nodes to trace the evolution of the pore surface. The differential equations governing the motion of the nodes were advanced in time using the second-order Runge–Kutta method with a variable time step that is proportional to the perimeter of the free surface. A complete simulation involving 500 time steps requires several hours of CPU time.

The results displayed in figure 6 reveal that the bubbles on the square lattice deform into rhomboidal shapes whose tip curvature continues to increase until a perfectly

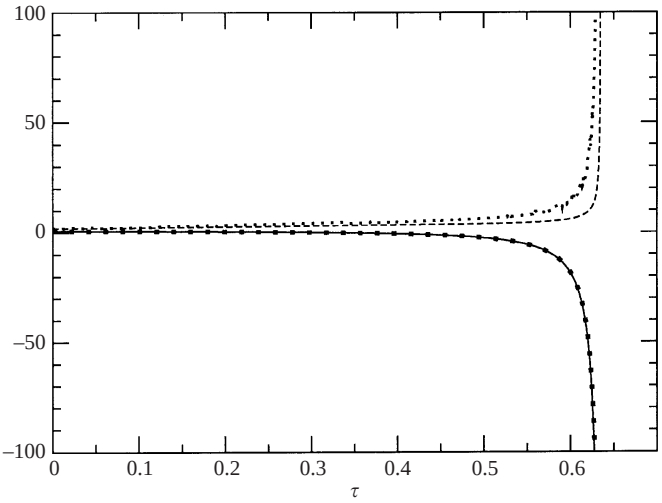

FIGURE 7. The solid and dashed curves display, respectively, the evolution of the reduced bubble pressure and minimum radius of curvature for the square lattice. The dotted lines display the corresponding evolution for the hexagonal lattice.

or nearly cuspidal shape develops, in agreement with the analytical predictions of Tanveer & Vasconcelos (1995) for solitary bubbles. In contrast, bubbles arranged on a hexagonal lattice maintain a nearly circular shape during the evolution. The difference between the two evolutions is attributed to the more pronounced spatial anisotropy of the square lattice that is responsible for strong deviations from the circular shape. Tanveer & Vasconcelos (1995) showed that interfacial waves are amplified during implosion due to shrinkage.

Figure 7 displays the evolution of the reduced bubble pressure $\delta\hat{p}_B \equiv (p_B - p_0)L_0^2/(\mu Q)$ and the corresponding evolution of the minimum radius of curvature reduced by L_0. The pressure inside a contracting solitary circular bubble of radius a can be computed by elementary analytical methods, and is found to be

$$p_B = p_0 + \frac{\gamma}{a} - \frac{\mu Q}{\pi a^2},$$

where $Q = \mathrm{d}(\pi a^2)/\mathrm{d}t$. For the conditions corresponding to figure 6, this formula predicts that the initial reduced bubble pressure is $\delta\hat{p}_B(t = 0) = 0.6503$. The numerical computations show that $\delta\hat{p}_B(t = 0) = 0.74145$ for the square lattice and 0.67208 for the hexagonal lattice. These comparisons reveal that periodicity has a significant effect on the developing bubble pressure. Figure 7 shows that, in agreement with the analytical predictions for solitary bubbles, the bubble pressure in the periodic configuration decreases in time and diverges toward negative infinity at the critical time $\tau_c = 0.636$ where the bubbles disappear.

Of particular interest is the evolution of a doubly periodic array of pores whose pressure is specified and the rate of expansion is computed as part of the solution. In the case of viscous sintering, the bubble pressure is typically assumed to be, and remain equal to, the equilibrium ambient pressure p_0. Figure 8 shows results of numerical simulations conducted using the first method discussed in § 2.3, for the square and hexagonal lattice. The initial condition is the same as that described earlier for the simulations depicted in figure 6. The labels above the frames show the dimensionless time $\tau \equiv \gamma t/(\mu L_0)$, where L_0 is the initial lattice side. In this case,

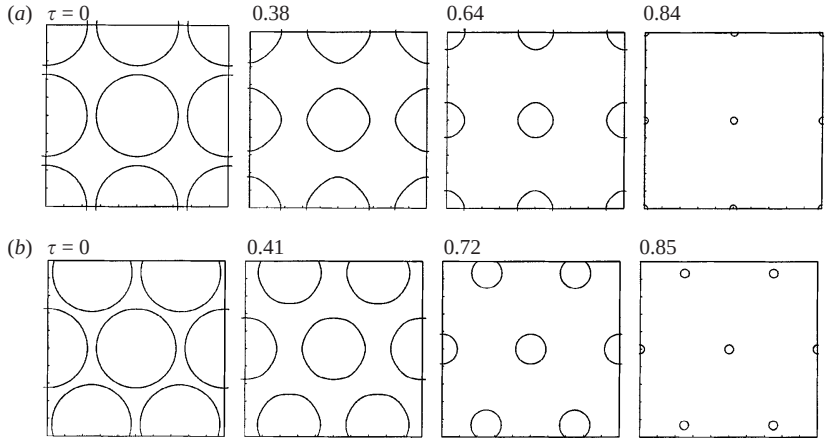

FIGURE 8. Evolution of shrinking constant-pressure pores on (*a*) a square and (*b*) a hexagonal lattice.

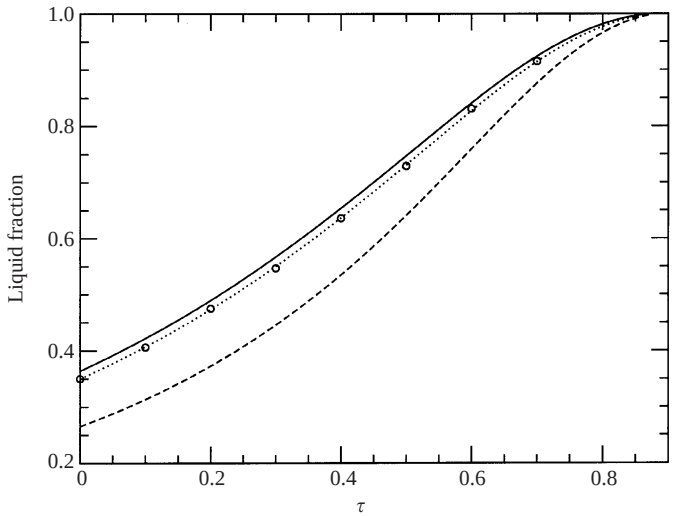

FIGURE 9. Evolution of the liquid fraction during densification due to the shrinkage of constant-pressure pores. The solid and dashed lines correspond, respectively, to the square and hexagonal lattice illustrated in figure 8. The circles represent data read off figure 3 of van de Vorst (1995) for a square lattice with initial liquid fraction 0.35, and the dotted line represents corresponding results obtained using the present formulation.

the interfaces remain smooth at all times and nearly cuspidal shapes do not develop. This variation underscores the importance of the rate of shrinkage not only for the qualitative but also for the qualitative features of the motion. Figure 9 shows the evolution of the liquid fraction toward the value of unity. The solid line corresponds to the square lattice, and the dashed line corresponds to the hexagonal lattice.

4.2. *Reciprocal theorem with a periodic lattice of point sources*

The dipole field defined in (4.3) satisfies the equations

$$\nabla \cdot \boldsymbol{D} = \sum_n \delta_2(\boldsymbol{x} - \boldsymbol{x}^{(n)}), \qquad \nabla^2 \boldsymbol{D} = 0, \tag{4.9}$$

and may thus be identified with the non-periodic velocity field induced by a doubly periodic array of point sources with unit strength, denoted by $u_i^s = D_i$; in (4.9), δ_2 is Dirac's delta function in the (x, y) plane. The associated pressure field is uniform throughout the domain of flow except at the singular points, and the associated stress field is given by $\sigma_{ij}^s = \mu\Sigma_{ij}$, where

$$\begin{aligned}\Sigma_{ij}(\boldsymbol{x}-\boldsymbol{x}_0) &= \left(\frac{\partial D_i}{\partial x_j}+\frac{\partial D_j}{\partial x_i}\right)(\boldsymbol{x},\boldsymbol{x}_0)\\ &= \frac{\delta_{ij}}{A_c}+\frac{1}{\pi}\sum_n \frac{1}{r_n^4}\left[\delta_{ij}r_n^2-2(1+\hat{r}_n^2)(x_i-x_i^{(n)})(x_j-x_j^{(n)})\right]\exp(-\hat{r}_n^2)\\ &\quad+\frac{2}{A_c}\sum_m \frac{k_i^{(m)}k_j^{(m)}}{k^{(m)^2}}\exp(-\tfrac{1}{4}\hat{k}^{(m)^2})\cos[\boldsymbol{k}^{(m)}\cdot(\boldsymbol{x}-\boldsymbol{x}_0)].\end{aligned} \tag{4.10}$$

It is worth noting that the velocity field $\boldsymbol{D}$ is related to the doubly periodic pressure Green's function of the two-dimensional Stokes flow, denoted by $\boldsymbol{p}$, by the equation

$$p_j(\boldsymbol{x}-\boldsymbol{x}_0) = 4\pi D_j(\boldsymbol{x}-\boldsymbol{x}_0)+\frac{2\pi}{A_c}(x_j-x_{0_j}), \tag{4.11}$$

as discussed in the Appendix.

Working as in § 2.2 for a solitary bubble, we derive an expression for the pore pressure in terms of integrals along the bubble surface C and contours of a unit cell I,

$$\begin{aligned}p_B &= \gamma\int_C D_i(\hat{\boldsymbol{x}})n_i(\boldsymbol{x})\kappa(\boldsymbol{x})\,\mathrm{d}l(\boldsymbol{x})-\mu\int_C u_i(\boldsymbol{x})\Sigma_{ij}(\hat{\boldsymbol{x}})n_j(\boldsymbol{x})\,\mathrm{d}l(\boldsymbol{x})\\ &\quad+\int_I D_i(\hat{\boldsymbol{x}})\sigma_{ij}(\hat{\boldsymbol{x}})n_j(\boldsymbol{x})\,\mathrm{d}l(\boldsymbol{x})-\mu\int_I u_i(\boldsymbol{x})\Sigma_{ij}(\hat{\boldsymbol{x}})n_j(\boldsymbol{x})\,\mathrm{d}l(\boldsymbol{x}),\end{aligned} \tag{4.12}$$

where $\hat{\boldsymbol{x}} = \boldsymbol{x}-\boldsymbol{x}_s$, $\boldsymbol{x}_s$ is the location of a periodically repeated point source situated in the pore interior, and the normal vector over I points into the cell.

In the absence of fluid motion, the second and fourth integrals on the right-hand side of (4.12) vanish. Using the integral identity (4.6), we find that the third integral is equal to the equilibrium liquid pressure p_0, as expected.

To eliminate the undesirable integrals along I on the right-hand side of (4.12), we decompose $\boldsymbol{D}$ and $\boldsymbol{\Sigma}$ into non-periodic components consisting of the first terms on the right-hand sides of (4.3) and (4.10), and remaining periodic components denoted by the superscript P. Taking advantage of the periodicity of the stress field and rearranging, we derive the equivalent expression

$$\begin{aligned}p_B &= \gamma\int_C D_i^P(\hat{\boldsymbol{x}})n_i(\boldsymbol{x})\kappa(\boldsymbol{x})\,\mathrm{d}l(\boldsymbol{x})-\mu\int_C u_i(\boldsymbol{x})\Sigma_{ij}^P(\hat{\boldsymbol{x}})n_j(\boldsymbol{x})\,\mathrm{d}l(\boldsymbol{x})\\ &\quad+\frac{1}{2A_c}\int_C \hat{x}_j[\sigma_{ji}(\boldsymbol{x})n_i(\boldsymbol{x})+p_Bn_j(\boldsymbol{x})]\,\mathrm{d}l(\boldsymbol{x})+\frac{1}{2A_c}\int_I \hat{x}_j\sigma_{ji}(\boldsymbol{x})n_i(\boldsymbol{x})\,\mathrm{d}l(\boldsymbol{x})\\ &\quad-\mu\left(\frac{Q}{A_c}+\int_I u_i(\boldsymbol{x})\Sigma_{ij}(\hat{\boldsymbol{x}})n_j(\boldsymbol{x})\,\mathrm{d}l(\boldsymbol{x})\right).\end{aligned} \tag{4.13}$$

Using the divergence theorem, we find that the third and fourth terms on the right-hand side of (4.12) are equal to the mean pressure over the area of the unit cell,

defined as

$$\bar{p} \equiv -\frac{1}{2A_c} \int_{cell} \sigma_{ii} \, \mathrm{d}x \, \mathrm{d}y, \tag{4.14}$$

where we have set $\sigma_{ij} = -p_B \delta_{ij}$ in the bubble interior. Moreover, because the structure of the lattice is assumed to be preserved, the tangential velocity is periodic along facing sides of the contour of the unit cell, whereas the normal velocity consists of a periodic component and a non-periodic component equal to $\boldsymbol{u}^P \cdot \boldsymbol{n} \equiv U_n = -Q/L_I$, where L_I is the perimeter of I. Expression (4.13) then simplifies to

$$p_B = \gamma \int_C D_i^P(\hat{\boldsymbol{x}}) n_i(\boldsymbol{x}) \kappa(\boldsymbol{x}) \, \mathrm{d}l(\boldsymbol{x}) - \mu \int_C u_i(\boldsymbol{x}) \Sigma_{ij}^P(\hat{\boldsymbol{x}}) n_j(\boldsymbol{x}) \, \mathrm{d}l(\boldsymbol{x}) + \bar{p} - \mu \frac{Q}{A_c} \left(1 - \frac{A_c}{L_I} \int_I n_i(\boldsymbol{x}) \Sigma_{ij}(\hat{\boldsymbol{x}}) n_j(\boldsymbol{x}) \, \mathrm{d}l(\boldsymbol{x}) \right). \tag{4.15}$$

It can be shown that the term enclosed by the large parentheses on the right-hand side of (4.15) is equal to 2, independent of the location of the point source.

When the bubble pressure p_B and average pressure $\bar{p}$ are required to be the same as the equilibrium reference pressure p_0 prevailing in the absence of fluid motion, equation (4.15) provides us with the integral constraint

$$\gamma \int_C D_i^P(\hat{\boldsymbol{x}}) n_i(\boldsymbol{x}) \kappa(\boldsymbol{x}) \, \mathrm{d}l(\boldsymbol{x}) - \mu \int_C u_i(\boldsymbol{x}) \Sigma_{ij}^P(\hat{\boldsymbol{x}}) n_j(\boldsymbol{x}) \, \mathrm{d}l(\boldsymbol{x}) - 2\mu \frac{Q}{A_c} = 0. \tag{4.16}$$

Van de Vorst (1995, 1996) implemented the method described in the second paragraph of § 2.3 using an essentially equivalent version of relation (4.16) as a constraint. In his formulation, the integrals over I were retained and the velocity along the contour of the unit cell was computed by solving an integral equation. The circles in figure 9 represent data read off figure 3 of van de Vorst (1995) for a square lattice with initial liquid fraction 0.35, and the dotted lines represent results' obtained using the method discussed in the last paragraph of § 4.1. The excellent agreement between the two simulations corroborates the consistency and equivalence of the two approaches.

5. Discussion

We have discussed methods for computing the bubble pressure in Stokes flow for three prototypical configurations. Other types of flow, including flow with multiple bubbles and flow past doubly or triply periodic suspensions of bubbles, may be treated by straightforward modifications of the basic formulation. The new methodology allows the practical computation of the bubble pressure with arbitrary precision in two-dimensional flow. Numerical error undermines the accuracy for three-dimensional flow and requires the use of refined grids that inflate the cost of the computation. These pragmatic constraints, however, are common in problems of three-dimensional interfacial flow.

Boundary-integral methods for simulating the deformation and shrinkage of constant-pressure compressible two-dimensional bubbles and pores in Stokes flow were developed and implemented by Power (1992), van de Vorst (1993), and Primo, Wrobel & Power (2000) for solitary configurations, and by van de Vorst (1995, 1996) and Pozrikidis (2002*a*) for doubly periodic flow. Van de Vorst and Pozrikidis used the direct formulation, whereas Power and Primo *et al.* used an indirect representation consisting a point source situated inside each pore to account for changes in the pore area and a single-layer Stokes potential whose density is computed by solving

an integral equation. Our discussion in § 4 for doubly periodic flow suggests that the method based on the potential dipole representation of the pressure is significantly more efficient than that based on the application of the reciprocal theorem with a point source.

The integral representations for the bubble pressure discussed in this paper can be generalized to Navier–Stokes and non-Newtonian flow. For example, applying the generalized reciprocal theorem for steady two-dimensional Newtonian flow with the flow due to the point source as a test flow (e.g. Pozrikidis 1997), and treating the inertial force as an effective body force, we find that the bubble pressure is given by the integral representation (2.13) where the right-hand side also includes the following integral computed over the domain of flow:

$$-\frac{1}{4\pi}\int\int_{Flow} P_i(\hat{\boldsymbol{x}})\frac{\partial \sigma_{ik}}{\partial x_k}(\hat{\boldsymbol{x}})\,\mathrm{d}A(\boldsymbol{x}). \tag{5.1}$$

In the case of Navier–Stokes flow, $\nabla\cdot\boldsymbol{\sigma} = \rho \mathrm{D}\boldsymbol{u}/\mathrm{D}t$, where ρ is the density and $\mathrm{D}/\mathrm{D}t$ is the material derivative. Note the first term on the left-hand side of (2.13) also arises from (5.1) by setting $\nabla\cdot\boldsymbol{\sigma} = \gamma\int_C \delta_2(\boldsymbol{x}-\boldsymbol{x}')\gamma(\boldsymbol{x}')\boldsymbol{n}(\boldsymbol{x}')\,\mathrm{d}l(\boldsymbol{x}')$, where $\delta_2(\boldsymbol{x}-\boldsymbol{x}')$ is Dirac's delta function in the (x, y)-plane. The implementation of this formulation to study the effect of fluid inertia on the pressure developing inside an incompressible bubble and on the rate of expansion of a compressible bubble is currently under investigation.

This research was supported in part by a grant provided by the National Science Foundation.

Appendix

To simulate the expansion or shrinkage of a doubly periodic lattice of bubbles or pores, we compute the motion of the interfaces using the method of interfacial dynamics for Stokes flow. As a preliminary, we introduce the doubly periodic Green's function of two-dimensional Stokes flow, denoted by $G_{ij}^{2D\text{-}2P}(\boldsymbol{x}, \boldsymbol{x}_0)$, representing the ith component of the velocity at the point $\boldsymbol{x}$ due to a lattice of point forces oriented along the jth axis, where one of the point forces is located at the point $\boldsymbol{x}_0$. The geometry of the point-force lattice corresponds to the instantaneous structure of the doubly periodic suspension. The corresponding Green's function for the stress is denoted by $T_{ijk}^{2D\text{-}2P}(\boldsymbol{x}, \boldsymbol{x}_0)$. Expressions for these Green's functions in terms of rapidly converging Ewald sums have been derived by van de Vorst (1996) and have been restated in adapted form by Pozrikidis (2001*b*, 2002*a*).

It is particularly significant to note that the velocity Green's function, $G_{ij}^{2D\text{-}2P}(\boldsymbol{x}, \boldsymbol{x}_0)$, is periodic in the directions of the two lattice vectors, whereas the stress Green's function, $T_{ijk}^{2D\text{-}2P}(\boldsymbol{x}, \boldsymbol{x}_0)$, consists of a linear non-periodic component and a remaining periodic component; the former expresses a linear pressure field necessary to balance the point forces underlying the Green's function. To emphasize this property, we write

$$T_{ijk}^{2D\text{-}2P}(\boldsymbol{x}, \boldsymbol{x}_0) = -\delta_{ik}\frac{4\pi}{A_c}(x_j - x_{0_j}) + T_{ijk}^{2D\text{-}2P\text{-}P}(\boldsymbol{x}, \boldsymbol{x}_0), \tag{A 1}$$

where the superscript $2D$-$2P$-P denotes the periodic component.

Consider the lattice illustrated in figure 5, and select as a control area the region occupied by the liquid in one unit cell. The boundary-integral formulation provides us with an expression for the velocity at a point $\boldsymbol{x}_0$ located inside the control area in

the integral form

$$u_j(\boldsymbol{x}_0) = -\frac{1}{4\pi\mu}\int_{C,I} f_i(\boldsymbol{x}) G_{ij}^{2D\text{-}2P}(\boldsymbol{x},\boldsymbol{x}_0)\,\mathrm{d}l(\boldsymbol{x}) + \frac{1}{4\pi}\int_{C,I} u_i(\boldsymbol{x}) T_{ijk}^{2D\text{-}2P}(\boldsymbol{x},\boldsymbol{x}_0) n_k(\boldsymbol{x})\,\mathrm{d}l(\boldsymbol{x}), \tag{A 2}$$

where I stands for the contour of the unit cell, and $\boldsymbol{f} \equiv \boldsymbol{\sigma}\cdot\boldsymbol{n}$ is the boundary traction (e.g. Pozrikidis 1992). Exploiting the periodicity of the stress field, the conforming periodicity of the Green's function for the velocity, and the opposite orientations of the normal vector over facing sides of I, we find that, because of cancellations, the single-layer potential expressed by the first integral on the right-hand side of (A 2) over I vanishes.

Next, we note that, because the structure of the lattice is preserved, the tangential velocity is periodic along facing sides of the contour of the unit cell, whereas the normal velocity can be decomposed into a periodic component and a constant non-periodic component component given by $\boldsymbol{u}^P\cdot\boldsymbol{n} \equiv U_n = -Q/L_I$, and L_I is the perimeter of I. Cancelling out the periodic contributions, enforcing the free-surface condition and rearranging, we obtain

$$u_j(\boldsymbol{x}_0) = -\frac{\gamma}{4\pi\mu}\int_C \kappa(\boldsymbol{x})\, n_i(\boldsymbol{x}) G_{ij}^{2D\text{-}2P}(\boldsymbol{x},\boldsymbol{x}_0)\,\mathrm{d}l(\boldsymbol{x}) + \frac{1}{4\pi}\int_C u_i(\boldsymbol{x}) T_{ijk}^{2D\text{-}2P}(\boldsymbol{x},\boldsymbol{x}_0) n_k(\boldsymbol{x})\,\mathrm{d}l(\boldsymbol{x}) - \frac{Q}{2A_c}\left(\frac{A_c}{2\pi L_I}\int_I n_i(\boldsymbol{x}) T_{ijk}^{2D\text{-}2P}(\boldsymbol{x},\boldsymbol{x}_0) n_k(\boldsymbol{x})\,\mathrm{d}l(\boldsymbol{x})\right). \tag{A 3}$$

It can be shown that the term enclosed by the large parentheses on the right-hand side of (A 3) is equal to x_{0_j}, yielding the simplified integral representation

$$u_j(\boldsymbol{x}_0) = -\frac{\gamma}{4\pi\mu}\int_C \kappa(\boldsymbol{x})\, n_i(\boldsymbol{x}) G_{ij}^{2D\text{-}2P}(\boldsymbol{x},\boldsymbol{x}_0)\,\mathrm{d}l(\boldsymbol{x}) + \frac{1}{4\pi}\int_C u_i(\boldsymbol{x}) T_{ijk}^{2D\text{-}2P}(\boldsymbol{x},\boldsymbol{x}_0) n_k(\boldsymbol{x})\,\mathrm{d}l(\boldsymbol{x}) - \frac{Q}{2A_c}x_{0_j}. \tag{A 4}$$

The physical interpretation of (A 4) becomes evident by decomposing the stress tensor into its pressure and velocity gradient constituents, and expressing the pressure Green's function in terms of the doubly periodic point source, as shown in (4.11). The result is

$$u_j(\boldsymbol{x}_0) = -\frac{\gamma}{4\pi\mu}\int_C \kappa(\boldsymbol{x})\, n_i(\boldsymbol{x}) G_{ij}^{2D\text{-}2P}(\boldsymbol{x},\boldsymbol{x}_0)\,\mathrm{d}l(\boldsymbol{x}) + \int_C D_j(\boldsymbol{x}_0-\boldsymbol{x}) u_k(\boldsymbol{x}) n_k(\boldsymbol{x})\,\mathrm{d}l(\boldsymbol{x}) + \frac{1}{4\pi}\int_C u_i(\boldsymbol{x})\left(\frac{\partial G_{ij}^{2D\text{-}2P}}{\partial x_k} + \frac{\partial G_{kj}^{2D\text{-}2P}}{\partial x_i}\right)(\boldsymbol{x}-\boldsymbol{x}_0) n_k(\boldsymbol{x})\,\mathrm{d}l(\boldsymbol{x}) - \frac{1}{2A_c}\int_C x_j u_k(\boldsymbol{x}) n_k(\boldsymbol{x})\,\mathrm{d}l(\boldsymbol{x}). \tag{A 5}$$

The four integrals on the right-hand side represent, respectively, interfacial distri-

butions of point forces, point sources, point-force dipoles, and a constant velocity expressing global translation.

Taking now the limit of (A 4) as the point $\boldsymbol{x}_0$ approaches the free surface, and expressing the limit of the double-layer potential in terms of its principal value, we obtain an integral equation of the second kind for the interfacial velocity,

$$u_j(\boldsymbol{x}_0) = -\frac{\gamma}{2\pi\mu}\int_C \kappa(\boldsymbol{x}) n_i(\boldsymbol{x}) G_{ij}^{2D\text{-}2P}(\boldsymbol{x},\boldsymbol{x}_0)\,\mathrm{d}l(\boldsymbol{x}) + \frac{1}{2\pi}\int_C^{PV} u_i(\boldsymbol{x})\, T_{ijk}^{2D\text{-}2P}(\boldsymbol{x},\boldsymbol{x}_0) n_k(\boldsymbol{x})\,\mathrm{d}l(\boldsymbol{x}) - \frac{Q}{A_c}x_{0_j}, \tag{A 6}$$

where PV denotes the principal value of the double-layer integral. Solving this integral equation allows us to advance the position of the interface.

The foregoing analysis may be modified to account for circumstances where the geometry of the lattice changes in a specified way during the motion. In such cases, the normal velocity along the contour of the unit cell can be decomposed into a periodic and a non-periodic component determining the change in the lattice geometry. The end result is the integral representation (A 4), where the last term on the right-hand side is replaced by a non-isotropic linear function whose divergence is equal to $-Q/A_c$.

REFERENCES

Crowdy, D. 2003*a* Compressible bubbles in Stokes flow. *J. Fluid Mech.* (to appear).

Crowdy, D. 2003*b* Viscous sintering of unimodal and bimodal cylindrical packings with shrinking pores. *Eur. J. Appl. Maths* (to appear).

Nédélec, J.-C. & Plachard, J. 1973 Une methode variationelle d'elements finis pour la resolution numerique d'un probleme exterieur dans R^3. *Revue Française d'Automatique, Informatique, Recherche Opérationelle: Analyse Numérique R3* **7**, 105–129.

Power, H. 1992 The low Reynolds-number deformation of a gas bubble in shear flow – a general approach via integral equations. *Engng Anal. Bound. Elem.* **9**, 31–37.

Pozrikidis, C. 1992 *Boundary Integral and Singularity Methods for Linearized Viscous Flow*. Cambridge University Press.

Pozrikidis, C. 1997 *Introduction to Theoretical and Computational Fluid Dynamics*. Oxford University Press.

Pozrikidis, C. 2001*a* Expansion of a compressible bubble in Stokes flow. *J. Fluid Mech.* **442**, 171–189.

Pozrikidis, C. 2001*b* Effect of surfactants on the stability and rheology of emulsions and foam. *J. Engng Maths* **41**, 237–258.

Pozrikidis, C. 2001*c* Interfacial dynamics for Stokes flow. *J. Comput. Phys.* **169**, 250–301.

Pozrikidis, C. 2001*a* Expansion of a two-dimensional foam. *Engng Anal. Bound. Elem.* **26**, 495–504.

Pozrikidis, C. 2002*b* *A Practical Guide to Boundary-Element Methods with the Software Library BEMLIB*. Chapman & Hall/CRC.

Primo, A. R. M., Wrobel, L. C. & Power, H. 2000 An indirect boundary-element method for slow viscous flow in a bounded region containing air bubbles. *J. Engng Maths* **37**, 305–326.

Richardson, S. 1968 Two-dimensional bubbles in slow viscous flow. *J. Fluid Mech.* **33**, 476–493.

Tanveer, S. & Vasconcelos, G. L. 1995 Time-evolving bubbles in two-dimensional Stokes flow. *J. Fluid Mech.* **301**, 325–344.

van de Vorst, G. A. L. 1993 Stokes flow with shrinking holes applied to viscous sintering. *J. Fluid Mech.* **257**, 667–689.

van de Vorst, G. A. L. 1995 Numerical simulation of viscous sintering by a periodic lattice of a representative unit cell. *RANA* 95-08. Eindhoven University of Technology.

van de Vorst, G. A. L. 1996 Integral formulation to simulate the viscous sintering of a two-dimensional lattice of periodic unit cells. *J. Engng Maths* **30**, 97–118.

Yan, Y. & Sloan, I. H. 1988 On integral equations of the first kind with logarithmic kernels. *J. Integral Equat. Applics.* **1**, 549–579.